PERGAMON

International Journal of Multiphase Flow 27 (2001) 1179–1198

International Journal of Multiphase Flow

www.elsevier.com/locate/ijmulflow

Linear instability of two-way coupled particle-laden jet

James DeSpirito, Lian-Ping Wang *

Department of Mechanical Engineering, 126 Spencer Laboratory, University of Delaware, DE 19716-3140, USA

Received 15 June 2000; received in revised form 14 November 2000

Abstract

The two-way coupled particle-laden jet is studied numerically in order to understand how the addition of solid particles affects the stability of the jet. In contrast with the particle-laden mixing layer studied, the jet flow stability is complicated by a variable wave (or phase) velocity and an additional curvature parameter, i.e., the ratio of jet radius to shear layer thickness. Nevertheless, we have demonstrated that the following similar scenario holds for a particle-laden jet: the addition of particles can destabilize the flow at small particle Stokes number, while the stabilizing effect prevails for intermediate to large Stokes numbers. Both these competing effects scale approximately linearly with the particle mass loading. We also found that the addition of particles increases the wave velocity at high wave numbers but decreases the wave velocity at low wave numbers. The fact that the addition of particles can destabilize the gas flow in the absence of gravity has been shown to follow the previous speculation. Two general asymptotic relations proposed by Saffman have been confirmed numerically for the case of the particle-laden jet. Physically, the increase of effective inertia of the fluid–particle mixture causes a destabilization effect while the enhanced viscous dissipation around the particles gives a stabilization effect. Results for various mass loadings, Stokes numbers, and wave numbers show that for a given mass loading and wave number, there is an intermediate Stokes number that corresponds to a maximum flow stability. We have shown that this Stokes number is on the order of 1 and depends weakly on the wave number.

Keywords: Particle-laden flow; Instability; Jet shear layer; Two-way coupling; Stokes number; Mass loading

1. Introduction

Particle-laden jet flows are commonly found in engineering applications ranging from jet propulsion, spray combustion, spray coating, and pulverized coal combustion. The mixing of small solid particles or liquid droplets with the gas phase determines the efficiency and stability of

* Corresponding author. Tel.: +1-302-831-8160; fax: +1-302-831-3619.
E-mail addresses: lwang@me.udel.edu, wang@bubble.me.udel.edu (L.-P. Wang).

0301-9322/01/$ - see front matter
PII: S0301-9322(00)00067-7

the particular process, e.g., droplet vaporization and mixing or contaminant removal. In these and other examples it is desirable to achieve a specific particle concentration profile. Therefore, the ability to predict and control particle dispersion in jet flow and other free shear flows is important to developing and improving designs of industrial equipment.

The evolution of the single-phase jet at high Reynolds number has been thoroughly studied in the past (e.g., Liu, 1989; Monkewitz and Pfizenmaier, 1991; Martin and Meiburg, 1991; Brancher et al., 1994). However, there are only a few studies on particle-laden jet flows, most of which address the problem of particle transport under the one-way coupling assumption (Chung and Troutt, 1988; Crowe et al., 1988, 1993; Hansell et al., 1992; Longmire and Eaton, 1992; Eaton and Fessler, 1994; Uthuppan et al., 1994; Aggarwal and Uthuppan, 1999; Glaze and Frankel, 2000). These studies have established that the effect of the large-scale structures on particle dispersion can be characterized in terms of the particle Stokes number, St, which is defined as the ratio of the particle aerodynamic response time to the timescale of the large-scale fluid motion (Crowe et al., 1988, 1993). Large-scale structures such as jet vortex rings can significantly influence the dispersion and mixing of particles in the jet if the Stokes number is on the order of 1.

Moderate mass loadings of particles can also alter the fluid flow, which is known as flow modulation (or turbulence modulation if the carrier flow is turbulent). In gas–solid flows, the particulate volume fraction may be low due to small particle sizes, but the mass loading can be on the order of 1 because of the high particle to fluid density ratio. In this case, the particles can significantly change the carrier flow characteristics, but particle–particle interactions may be neglected (Elghobashi, 1994). This two-way coupling regime is of concern in this study. Turbulence or flow modulation by particles has been known for several decades. The issue of whether turbulence in the carrier flow is enhanced or reduced by the dispersed particles has been the subject of experimental studies (e.g., Gore and Crowe, 1989, 1991; Hetsroni, 1989), theoretical model development (Yuan and Michaelides, 1992; Yarin and Hetsroni, 1994; Crowe et al., 1997), and direct numerical simulations (Squires and Eaton, 1990; Elghobashi and Truesdell, 1993; Tong and Wang, 1999).

Shear flows usually develop from linear instabilities and as such the study of instability of the particle-laden jet would be the first step towards a better understanding of two-way coupled evolution of a two-phase jet. Studies of instability of particle-laden shear flows have primarily focused on the inviscid mixing layer (Michael, 1965; Yang et al., 1990; Wen and Evans, 1994; Dimas and Kiger, 1998) with limited study of the viscous mixing layer (Saffman, 1962; Tong and Wang, 1999). Instability studies of the particle-laden jet have been limited to the inviscid case (Sykes and Lyell, 1994; Parthasarathy, 1995). Sykes and Lyell (1994) studied the spatial stability of an inviscid two-phase circular jet and found the particles to have a stabilizing effect. The spatial growth rate was found to decrease for both the axisymmetric and first azimuthal modes. They also found that, for both perturbation modes, the addition of particles increased the phase velocity of the perturbation above the most amplified frequency. Below this frequency the addition of particles decreased the phase velocity. Parthasarathy (1995) studied both the spatial and temporal stabilities of the circular particle-laden jet. The axisymmetric and first azimuthal modes were investigated. The temporal stability analysis of a particle-laden top-hat jet indicated that particles decreased the wave amplification but increased the wave velocity, with both effects increasing with particle loading. The spatial stability analysis showed that the presence of particles decreased the amplification rate at all frequencies. The phase velocity of the particle-laden flow disturbances was

smaller than that of the single-phase flow at low frequencies. At frequencies higher than the single-phase maximum-amplified frequency, the phase velocity of the particle-laden flow disturbance was higher.

In this paper, we investigate the temporal stability of a viscous, two-way coupled particle-laden, axisymmetric jet flow. A finite difference direct numerical simulation code was used to determine the temporal growth rate of the imposed disturbance. This study extends the work of Tong and Wang (1999) on the two-way coupled particle-laden mixing layer. The instability characteristics of the jet are compared to that of the mixing layer, as a way of validating our numerical method. The asymptotic behaviors proposed by Saffman (1962) were shown to hold for the jet flow in this study. The paper is organized as follows: in Section 2, we present the mathematical formulation and theoretical predictions; the numerical method is described in Section 3; and numerical results are discussed and compared with theories in Section 4.

2. Theory

We consider an axisymmetric gas jet shear layer with solid particles in which the volume fraction of the particulate phase is very low, as such effects of particle concentrations on continuous phase viscosity are small. The particles are uniform in size with diameter much smaller than any characteristic length scales in the base gas flow. The particle density is much larger than that of the gas ($\rho_p/\rho_f \gg 1$) so that the bulk mass loading of the particulate phase is on the order of 1. As such, the flow modulation by the particles may be significant. Also because of the large density ratio, effects of virtual mass, Basset histoy forces, etc., can be neglected. The particle Reynolds numbers are in the Stokes flow region so that linear Stokes drag is assumed, as in the previous studies of Saffman (1962), Parthasarathy (1995), and Tong and Wang (1999). The dimensional governing equations for the carrier gas (subscript f) and the particulate phase (subscript p) of the axisymmetric jet are

$$\nabla \cdot \mathbf{u} = 0, \tag{1}$$

$$\frac{\partial \mathbf{u}}{\partial t} + \mathbf{u} \cdot \nabla \mathbf{u} = \frac{1}{\rho_f} \nabla P - \frac{3\pi\mu n d}{\rho_f} (\mathbf{u} - \mathbf{v}) + \nu \nabla^2 \mathbf{u}, \tag{2}$$

$$\frac{\partial \epsilon}{\partial t} + \nabla \cdot (\epsilon \mathbf{v}) = 0, \tag{3}$$

$$\frac{\partial \mathbf{v}}{\partial t} + \mathbf{v} \cdot \nabla \mathbf{v} = \frac{18\mu}{\rho_p d^2} (\mathbf{u} - \mathbf{v}), \tag{4}$$

where $\mathbf{u} \equiv (u_r, u_z)$ is the gas velocity, $\mathbf{v} \equiv (v_r, v_z)$ is the particle velocity, P is the gas pressure, ρ_f is the gas density, and ρ_p is the particle velocity. The momentum coupling is described by the term $(3\pi\mu n d)/\rho_f(\mathbf{u} - \mathbf{v})$, where n is the particle number density and d is the particle diameter, μ and ν are the gas dynamic and kinematic viscosity, respectively. The particle local volume fraction, ϵ, is related to the number density as $\epsilon = n\pi d^3/6$.

The above mathematical formulation, known as the continuum approach, is identical to that proposed in Saffman (1962) paper. Although the validity of the continuum approach for larger St numbers may be questionable for non-linear particle-laden shear layers in general (e.g., Slater and Young, 1998), the problems associated with the continuum approach are not present at the linear growth stage. We believe that the Eulerian approach gives consistent results in the limit of small mass loading, as long as the problem of linear instability is concerned. For further discussions, the reader is referred to the work of Slater and Young (1998).

The governing equations are now non-dimensionalized using the velocity of the gas at the centerline of the jet, U_0, the radius of the jet core, r_0, and an average particle volume fraction, ϵ_0. The non-dimensional equations for the gas and particulate phase become

$$\nabla \cdot \mathbf{u} = 0, \tag{5}$$

$$\frac{\partial \mathbf{u}}{\partial t} + \mathbf{u} \cdot \nabla \mathbf{u} = -\nabla P + \frac{\nabla^2 \mathbf{u}}{Re} - Z\epsilon \frac{[\mathbf{u} - \mathbf{v}]}{St}, \tag{6}$$

$$\frac{\partial \epsilon}{\partial t} + \nabla \cdot (\epsilon \mathbf{v}) = 0, \tag{7}$$

$$\frac{\partial \mathbf{v}}{\partial t} + \mathbf{v} \cdot \nabla \mathbf{v} = \frac{[\mathbf{u} - \mathbf{v}]}{St}, \tag{8}$$

where the same symbols are used to denote the corresponding non-dimensional variables. The flow Reynolds number, Re, is defined as $r_0 U_0/v$. In the flow momentum coupling term, Z is the average particle mass loading ($Z = \epsilon_0 \rho_p/\rho_f$); the Stokes number, St, represents the ratio of the particle response time ($\tau_p = \rho_p d^2/18 v \rho_f$) to flow characteristic time ($\tau_f = r_0/U_0$). We note that an alternative definition for the flow characteristic time is $\tau_f^a = \delta/U_0$, where δ is the vorticity thickness of the initial jet shear layer ($\delta \equiv U_0/(\mathrm{d}U^*/\mathrm{d}r)|_{r=r_0}$) with $U^*(r)$ being the jet mean velocity profile. Therefore, $St^a \equiv \tau_p/\tau_f^a = St * \ r_0/\delta$. Here r_0/δ is an important parameter that measures the curvature effect on the jet flow.

Perhaps a more relevant flow characteristic time would be based on the dominant frequency associated with the jet instability (Aggarwal, 1994; Aggarwal and Uthuppan, 1999), namely, $\tau_f^b = \lambda/U_p = 2\pi r_0/(U_p \alpha)$, where α and λ are the instability wave number and wavelength, respectively; U_p is the phase velocity. For the most unstable axisymmetric instability wave, $\alpha \approx 2.2$ and $U_p \approx 0.6 U_0$. Therefore, $\tau_f^b \approx= 4.76\tau_f$. The Stokes number defined based on τ_f^b would then be about 21% the value of the Stokes number used in this paper.

The dimensionless mean velocity profile of the gas phase is assumed to be

$$U(r) \equiv \frac{U^*(r)}{U_o} = \frac{1}{2}\left\{1.0 + \tanh\left[\frac{2r_0}{\delta}(1.0 - r)\right]\right\}. \tag{9}$$

This profile was used in the previous studies of the single-phase axisymmetric jet (e.g., Michalke, 1984; Brancher et al., 1994). For the purpose of comparing our results with those of Tong and Wang (1999), we also used the following mean flow profile

$$U(r) = \frac{1}{2}\left\{1.0 + \mathrm{erf}\left[\sqrt{\pi}\frac{r_0}{\delta}(1.0 - r)\right]\right\}. \tag{10}$$

This profile was only used for the results to be discussed in Figs. 2 and 3.

The particles were initially distributed uniformly throughout the flow [$\epsilon(\bar{x}, t = 0) = 1$] with the initial particulate mean velocity equal to the fluid mean velocity. This assumption of dynamic equilibrium was used in the previous studies by Saffman (1962), Yang et al. (1990) and Tong and Wang (1999). The perturbation was taken to be periodic in the streamwise (z) direction and was unbounded in the radial direction with vanishing velocity perturbation at infinity. A finite difference method, presented in Section 3, was developed to solve the governing equations.

In this paper, we consider the temporal instability of an axisymmetric jet flow. Noting that experimental jet flows should be studied as a spatially developing problem (e.g., Huerre and Monkewitz, 1985), the observations to be made in this paper should only be valid qualitatively when considering a spatially evolving, viscous, particle-laden jet flow.

The system of equations (5)–(8) are linearized using perturbations of the form $B\,\mathrm{e}^{\mathrm{i}\,\alpha(z-ct)}$, where α is the perturbation wave number; c is the complex phase velocity; and B is $\hat{p}(r)$, $\hat{u}_r(r)$, $\hat{u}_z(r)$, $\hat{v}_r(r)$, $\hat{v}_z(r)$ or $\hat{\epsilon}(r)$, the eigenfunction for pressure, fluid radial or axial velocity, particulate radial or axial velocity or particulate volume fraction, respectively. Assuming that the perturbation stream function for the gas flow is of the form $\phi(r)\,\mathrm{e}^{\mathrm{i}\,\alpha(z-ct)}$, the Orr–Sommerfeld equation for a particle-laden, axisymmetric jet flow is found to be

$$\left[D^2 - \frac{1}{r}D - \alpha^2\right]^2 \phi = \mathrm{i}\,\alpha Re\left[(\overline{u} - c)\left(D^2 - \frac{1}{r}D - \alpha^2\right)\phi - \phi D^2\overline{u} + \frac{\phi}{r}D\overline{u}\right], \tag{11}$$

where $D \equiv \mathrm{d}/\mathrm{d}r$ and, as was shown by Saffman (1962), the usual mean flow $U(r)$ is replaced by a complex mean flow, $\overline{u}(r)$, in the presence of particles,

$$\overline{u}(r) = U(r) + \frac{Z(U - c)}{1 + \mathrm{i}\,\alpha(U - c)\,St}. \tag{12}$$

Comparing Eq. (11) with the Orr–Sommerfeld equation for a particle-laden plane mixing layer flow derived by Saffman (1962),

$$\left[D^2 - \alpha^2\right]^2 \phi = \mathrm{i}\,\alpha Re\left[(\overline{u} - c)\left(D^2 - \alpha^2\right)\phi - \phi D^2\overline{u}\right], \tag{13}$$

where now $D \equiv \mathrm{d}/\mathrm{d}y$, we see that Eq. (11) correctly approaches that of the plane shear layer as the ratio $r_0/\delta \to \infty$ since the mean flow shear occurs mainly in the region $1 - \delta/r_0 < r < 1 + \delta/r_0$. The mixing layer is a 4-parameter system, $\mathscr{F}(Re, \alpha, St, Z)$, while the jet is a 5-parameter system, $\mathscr{F}(Re, \alpha, St, Z, r_0/\delta)$. We will compare results for the two shear flows in Section 4.

For given initial mean velocity profiles, Eq. (11) represents an eigenvalue problem involving five governing parameters. The growth rate of a temporal instability mode, $\sigma \equiv \alpha c_\mathrm{i}$, is a function of the flow Reynolds number, Re, perturbation wave number, α, particle inertial parameter, St, particle mass loading, Z, and the curvature parameter, r_0/δ:

$$\sigma = \sigma\left(Re, \alpha, \frac{r_0}{\delta}, St, Z\right), \tag{14}$$

where c_i is the imaginary part of c. This compares to the growth rate, σ_0 for a single-phase jet, which is only a function of Re, α, and r_0/δ:

$$\sigma_0 = \sigma_0\left(Re, \alpha, \frac{r_0}{\delta}\right). \tag{15}$$

The real part of c is the phase (or wave) velocity, which, unlike that of the plane mixing layer investigated by Tong and Wang (1999), will be non-zero and vary with the system parameters. Since Eq. (7) is linear in ϵ, the perturbation field of the particle concentration can be determined, a posteriori, in terms of the eigenfunctions of the velocity fields.

Saffman (1962) made two important observations regarding the asymptotic solutions in terms of St. For the case of very fine particles, or $St \ll 1$, Saffman used a leading-order solution for the particle velocity field to show that the effect of the fine particles is equivalent to increasing the density of the mixture, and thus an increase of the flow Reynolds number by a factor of $(1+Z)$. A relation between the growth rate in particle-laden jet, σ, and that of the clean gas jet, σ_0, therefore exists:

$$\sigma\left(\alpha, Re, \frac{r_0}{\delta}, Z, St \ll 1\right) = \sigma_0\left[\alpha, Re_e = Re(1+Z), \frac{r_0}{\delta}\right]. \tag{16}$$

In this case, the addition of particles destabilizes the flow, since the growth rate of a singe-phase jet was shown to increase with Re (Michalke, 1984). This asymptotic relation implies a prediction of the two-phase instability in terms of single-phase instability in the limit of $St \ll 1$. This relation was confirmed for the viscous plane mixing layer by Tong and Wang (1999). We will compare this relation with numerical results for the viscous axisymmetric jet in Section 4.

In the limit of very large particle inertia, or $St \gg 1$, Saffman found that $\overline{u}(r) = U(r) - \mathrm{i}Z/(\alpha \cdot St)$ from Eq. (12). Eq. (11) can then be written in the same format as the single-phase Orr–Sommerfeld equation if $c_\mathrm{i} + Z/(\alpha \cdot St)$ is viewed as c_i in the single-phase flow. Then

$$\sigma\left(\alpha, Re, \frac{r_0}{\delta}, Z, St \gg 1\right) = \sigma_0\left(\alpha, Re, \frac{r_0}{\delta}\right) - \frac{Z}{St}, \tag{17}$$

which indicates that the growth rate decreases linearly with the loading for large St. We will confirm this numerically for the viscous jet in Section 4.

3. Numerical method

Normally, the Orr–Sommerfeld equation is solved numerically to obtain the growth rate and eigenfunctions of linear instability modes (e.g., Dimas and Kiger, 1998). Alternatively, they can be extracted from a numerical code designed to solve the full non-linear equations (5)–(8). The numerical scheme for the jet flow and the procedure for calculating linear instability are described here.

A finite difference code was developed to solve the three-dimensional, non-linear equations of motion for the carrier fluid and particulate phase. The finite difference code solved the governing equations in cylindrical coordinates using a staggered grid and fractional step method described by Kim and Moin (1985). Following the method of Rai and Moin (1991), a third-order Runge–Kutta method was used for the non-linear terms while the second-order Crank–Nicolson method was used for the linear (viscous) terms. The novel cylindrical coordinate formulation of Verzicco and Orlandi (1996) was used to handle the singularities at $r = 0$. The Poisson solver for the pressure equation used Fourier series expansions in the streamwise direction. This makes the

Poisson solver very efficient, but the periodic boundary condition in the streamwise direction currently limits the code to the solution of the temporally evolving jet.

Following Verzicco and Orlandi (1996), we replaced the primitive variables of the carrier flow, $\mathbf{u} = [u_r, u_z]^{\mathrm{T}}$, with the modified variables $\mathbf{q} = [q_r, q_z]^{\mathrm{T}}$, where $q_r = ru_r$ and $q_z = u_z$. In the staggered grid formulation, q_r is identically 0 at the axis and the terms with $1/r$, $1/r^2$, and $1/r^3$ in them can be properly defined near $r = 0$ when the momentum equations are written in the form given in the following. The carrier flow continuity equation, in the modified variables becomes

$$\frac{\partial q_r}{\partial r} + r\frac{\partial q_z}{\partial z} = 0, \tag{18}$$

and the carrier fluid momentum equations become

$$\frac{Dq_r}{Dt} = -r\frac{\partial p}{\partial r} + \frac{1}{Re}\left[r\frac{\partial}{\partial r}\left(\frac{1}{r}\frac{\partial q_r}{\partial r}\right) + \frac{\partial^2 q_r}{\partial z^2}\right] - Z\epsilon\frac{q_r - Q_r}{St}, \tag{19}$$

$$\frac{Dq_z}{Dt} = -\frac{\partial p}{\partial z} + \frac{1}{Re}\left[\frac{1}{r}\frac{\partial}{\partial r}\left(r\frac{\partial q_z}{\partial r}\right) + \frac{\partial^2 q_r}{\partial z^2}\right] - Z\epsilon\frac{q_z - Q_z}{St}, \tag{20}$$

with

$$\frac{Dq_r}{Dt} \equiv \frac{\partial q_r}{\partial t} + \frac{\partial}{\partial r}\left(\frac{q_r^2}{r}\right) + \frac{\partial(q_r q_z)}{\partial z}, \tag{21}$$

and

$$\frac{Dq_z}{Dt} \equiv \frac{\partial q_z}{\partial t} + \frac{1}{r}\frac{\partial(q_r q_z)}{\partial r} + \frac{\partial q_z^2}{\partial z}. \tag{22}$$

The particle momentum and continuity equations were written in a similar manner, with the modified variables $Q_r = rv_r$ and $Q_z = v_z$.

Using the third-order Runge–Kutta and second-order Crank–Nicolson scheme, the intermediate velocity value of the fractional step method is calculated from

$$\frac{\widehat{q}_{\mathrm{i}} - q_{\mathrm{i}}^l}{\Delta t} = \left[\gamma_l H_{\mathrm{i}}^l + \rho_l H_{\mathrm{i}}^{l-1} - \alpha_l \mathscr{G}_{\mathrm{i}} p^l + \alpha_l (A_{\mathrm{i}r} + A_{\mathrm{i}z})\frac{(\widehat{q}_{\mathrm{i}} + q_{\mathrm{i}}^l)}{2} + \alpha_l S_{\mathrm{i}}^l\right], \tag{23}$$

where H_{i} contains the convective terms and those viscous terms with a single velocity derivative; $\mathscr{G}_{\mathrm{i}}$, $A_{\mathrm{i}r}$, and $A_{\mathrm{i}z}$ denote discrete, second-order central differential relations for the pressure and viscous terms, respectively; and γ, ρ, and α are the Runge–Kutta coefficients. The force coupling term is treated as a source term, S_{i}^l. An approximate factorization method is used to reduce the problem to one of solving two tri-diagonal systems of equations:

$$(1 - \beta_l A_{\mathrm{i}r})(1 - \beta_l A_{\mathrm{i}z})\Delta\widehat{q}_{\mathrm{i}} = \Delta t\left[\gamma_l H_{\mathrm{i}}^l + \rho_l H_{\mathrm{i}}^{l-1} - \alpha_l \mathscr{G}_{\mathrm{i}} p^l + \alpha_l (A_{\mathrm{i}r} + A_{\mathrm{i}z}) q_{\mathrm{i}}^l + \alpha_l S_{\mathrm{i}}^l\right], \tag{24}$$

where $\Delta\hat{q} = \widehat{q}_{\mathrm{i}} - q_{\mathrm{i}}^l$ and $\beta_l = \alpha_l \Delta t/2$. Continuity is enforced to obtain the velocity at the next time step by

$$q_{\mathrm{i}}^{l+1} - \widehat{q}_{\mathrm{i}} = -\alpha_l \Delta t \mathscr{G}_{\mathrm{i}} \Phi^{l+1}, \tag{25}$$

where $\mathscr{G}$ is the gradient operator and Φ is a scalar field calculated from

$$\mathscr{L}\Phi^{l+1} = +\frac{1}{\alpha_l \Delta t}\mathscr{D}\hat{\mathbf{q}}, \tag{26}$$

where $\mathscr{L}$ and $\mathscr{D}$ represent the discrete Laplacian and divergence operators, respectively. The pressure is calculated from

$$p^{l+1} = p^l + \Phi^{l+1} - \left(\frac{\alpha_l \Delta t}{2Re}\right)\mathscr{L}\Phi^{l+1}. \tag{27}$$

After the fluid velocity was advanced in each Runge–Kutta step, the particulate momentum and continuity equations were solved in a similar manner, except that the pressure correction substep was not needed.

For the linear instability study, we first decomposed the velocity and particle volumetric concentration fields into the mean and disturbance fields:

$$\mathbf{u} = \begin{pmatrix} 0 \\ U(r) \end{pmatrix} + A(t)\begin{pmatrix} \hat{u}_{r\,\mathrm{R}}(r) + \mathrm{i}\,\hat{u}_{r\,\mathrm{I}}(r) \\ \hat{u}_{z\,\mathrm{R}}(r) + \mathrm{i}\,\hat{u}_{z\,\mathrm{I}}(r) \end{pmatrix} \mathrm{e}^{\mathrm{i}\,\alpha z}, \tag{28}$$

$$\mathbf{v} = \begin{pmatrix} 0 \\ U(r) \end{pmatrix} + A(t)\begin{pmatrix} \hat{v}_{r\,\mathrm{R}}(r) + \mathrm{i}\,\hat{v}_{r\,\mathrm{I}}(r) \\ \hat{v}_{z\,\mathrm{R}}(r) + \mathrm{i}\,\hat{v}_{z\,\mathrm{I}}(r) \end{pmatrix} \mathrm{e}^{\mathrm{i}\,\alpha z}, \tag{29}$$

$$\epsilon = 1 + A(t)[\hat{\epsilon}_{\mathrm{R}}(r) + \mathrm{i}\,\hat{\epsilon}_{\mathrm{I}}(r)]\,\mathrm{e}^{\mathrm{i}\,\alpha z}, \tag{30}$$

where the subscripts R and I denote the real and imaginary parts of the eigenfunctions, respectively, and $A(t)$ denotes the perturbation amplitude.

To determine the initial eigenfunctions to be used, the stream function representation for the perturbation field of the carrier flow was used to ensure incompressibility

$$\Psi(r,z) = Re\left[\phi(r)\,\mathrm{e}^{\mathrm{i}\,\alpha z}\right] = \phi_{\mathrm{R}}(r)\cos\alpha z - \phi_{\mathrm{I}}(r)\sin\alpha z, \tag{31}$$

where $\phi(r) = \phi_{\mathrm{R}}(r) + \mathrm{i}\,\phi_{\mathrm{I}}(r)$. The following initial forms of $\phi(r)$ were used:

$$\phi_{\mathrm{R}} = \frac{A_0}{\cosh^2\frac{r_0}{2}(1-r)}, \tag{32}$$

$$\phi_{\mathrm{I}} = \frac{A_0 \sinh\frac{r_0}{2}(1-r)}{\cosh^3\frac{r_0}{2}(1-r)}. \tag{33}$$

From the stream function, the initial velocity field in the modified variables are

$$q_z = U(r) - \frac{1}{r}[\phi'_{\mathrm{R}}\cos\alpha z - \phi'_{\mathrm{I}}\sin\alpha z], \tag{34}$$

$$q_r = -\alpha\phi_{\mathrm{R}}\sin\alpha z - \alpha\phi_{\mathrm{I}}\cos\alpha z, \tag{35}$$

where the primes in Eq. (34) now denote differentiation with respect to r.

The flow was advanced in time with the perturbation amplitude, $A(t)$, kept below 1% throughout the simulation to ensure linear instability behavior. The updated eigenfunctions were then used to specify the initial flow for the next iteration. This iteration procedure continued until all the eigenfunctions converged and $A(t)$ varied exponentially with time.

The exponential growth rate of the perturbation field was computed as

$$\sigma = \frac{\ln\left[\frac{A(t=\Delta t)}{A(t=0)}\right]}{\Delta t}. \tag{36}$$

The growth rate remains the same for new iterations once the eigenfunctions converge. The time development of the perturbation amplitude at the converged stage, under different mass loadings, is shown in Fig. 1 on a log-linear plot, with the slope being the growth rate, σ.

4. Results

4.1. Comparison with mixing layer: the curvature effect

The effect of the parameter r_0/δ on the jet instability was studied first to examine the curvature effect. Comparisons with the mixing layer results of Tong and Wang (1999) in the limit of large r_0/δ also serve as a validation tool for the jet flow code. In the mixing layer case, the only length scale is the shear layer thickness, which was taken to be the vorticity thickness, δ. Recognizing that the velocity scale used in the mixing layer is $\Delta U/2$ (ΔU is the velocity jump across the shear layer) and that different length scales exist, the parameters defined in this paper are related to those in Tong and Wang (1999), denoted by the 'mix' subscript, as follows:

$$Re = 2\left(\frac{r_0}{\delta}\right)Re_{\mathrm{mix}}, \quad St = 2\left(\frac{\delta}{r_0}\right)St_{\mathrm{mix}}, \quad Z = Z_{\mathrm{mix}}, \quad \alpha = \left(\frac{r_0}{\delta}\right)\alpha_{\mathrm{mix}}. \tag{37}$$

We shall compare with the mixing layer results at $Re_{\mathrm{mix}} = 250$, $St_{\mathrm{mix}} = 1.0$, $Z_{\mathrm{mix}} = 1.0$, and $\alpha_{\mathrm{mix}} = 0.862$. With these parameters given, Eq. (37) was used to determine the parameters used for

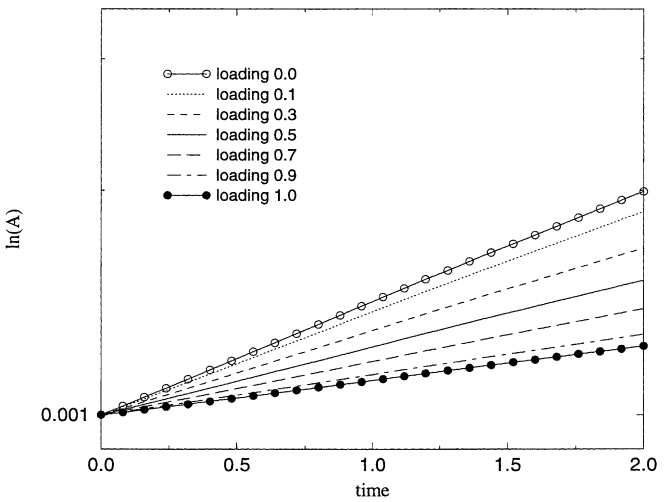

Fig. 1. Time development of perturbation amplitude at converged stage ($\alpha = 2.0$, $Re = 500$, $St = 1.0$, and $r_0/\delta = 2.825$).

the jet case once the curvature parameter, r_0/δ, was chosen. We varied r_0/δ from 2 to 32 and as such the wave number, α, varied from 1.724 to 27.58. Fig. 2 shows the dimensionless growth rate divided by the curvature parameter, $\sigma/(r_0/\delta) = \sigma_{\mathrm{mix}}/2$, versus the curvature parameter, r_0/δ, along with the growth rate for the mixing layer. We expect that the growth rate for the jet in the limit of large r_0/δ be the same as the mixing layer. Fig. 2 shows that the curvature significantly affects the growth rate only for $r_0/\delta < 4$. The maximum difference between the two growth rates is about 6% for $r_0/\delta > 5$, which may be caused by the finite domain size in the simulation. Fig. 3 shows the same comparison for the single-phase case. The jet growth rate approaches the mixing layer value a little slower than the particle-laden case but has reached the asymptote by $r_0/\delta = 8$. The maximum difference between the two growth rates is about 4% for $r_0/\delta > 8$. In summary, the curvature effect reduces the growth rate and suppresses the flow instability, as shown, for example, in the work of Martin and Meiburg (1991).

4.2. Reynolds number

We focused our study on the effects of α, St, and Z, with the understanding that the flow Reynolds number, Re, only modifies slightly the growth rate if Re is larger than, say, 1000. In Fig. 4, the variation of growth rate and phase velocity as a function of Reynolds number for the single-phase jet and a particle-laden jet are shown. The results were obtained by the numerical solution of Eqs. (18)–(20) along with that of appropriate particle equations, as explained in Section 3. The growth rate increases with Reynolds number quickly when $Re < 1000$ and gradually approaches the asymptotic value when Re is further increased. When $Re = 10,000$, the growth rate for the single-phase jet is 0.428, which is close to the inviscid growth rate of 0.449 (P.J. Morris, Private communication, see also Morris, 1976). The phase velocity decreases slightly from 0.628 at $Re = 100$ to 0.613 at $Re = 10,000$, almost independent of Reynolds number. A similar variation of the growth rate and phase velocity was found for the particle-laden jet. The effect of particles,

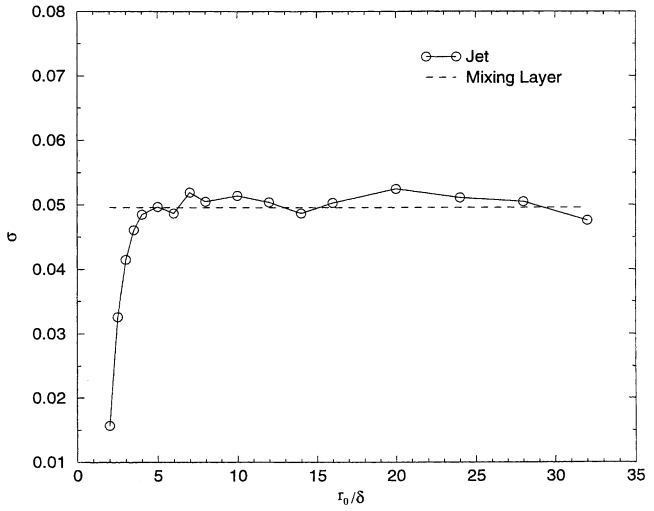

Fig. 2. Comparison of jet and mixing layer growth rates for particle-laden jet, $Z = 1.0$.

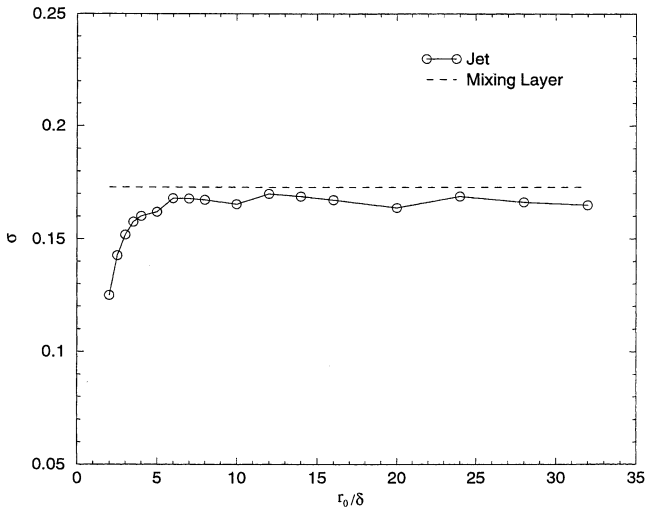

Fig. 3. Comparison of jet and mixing layer growth rates for single-phase jet.

at $Z = 1.0$ and $St = 1.0$, is to reduce the growth rate and increase the phase velocity. Since we are mainly interested in the effects of particle parameters on the flow instability, in the remaining sections we set $r_0/\delta = 2.825$ and $Re = 500$.

4.3. Effects of mass loading and Stokes number

The growth rate as a function of the particle mass loading for four different Stokes numbers and $\alpha = 2.0$ is shown in Fig. 5. The single-phase growth rate is also shown in the figure. For large Stokes number ($St = 10$), the growth rate decreases linearly with increasing Z with a slope of about $1/St$, as predicted by Saffman (1962). The dependence on loading is not linear for the small and intermediate Stokes numbers. For the smallest Stokes number ($St = 0.01$), the growth rate is shown to be higher than that for a single-phase flow, increasing slowly with loading. In this case the addition of particles actually destabilizes the flow, as predicted by Saffman (1962). For a given α and Z, the flow is most stable for St on the order of 1, due to the most effective fluid-to-particle interphase energy transfer as discussed in Tong and Wang (1999). The gas flow gives away energy to the particulate phase, leading to a slower instability growth of the jet.

Fig. 6 shows the growth rate and phase velocity as a function of wave number for $St = 1$ and three loadings. The addition of particles always has a stabilizing effect at this Stokes number and the stabilizing effect is shown to increase with loading. There is a most unstable wave number at each loading, with the most unstable wave number decreasing with increasing loading. This indicates that heavy loading will lead to roll-up at longer wavelength. The phase velocity shows the largest variation with wave number, particularly at small wave numbers. The long-wave perturbations propagate at close to jet center velocity, while short-wave perturbations may travel at about 60% of the jet velocity. The loading seems to decrease the phase velocity of long-wave perturbations but increase that of short-wave perturbations, in agreement with the results of

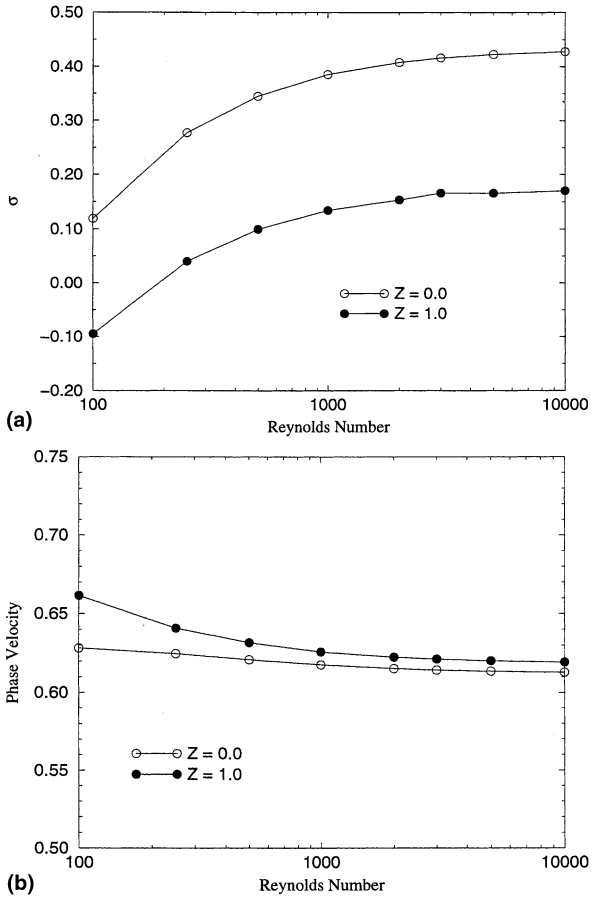

Fig. 4. Growth rate (a) and phase velocity (b) of single-phase and particle-laden ($Z = 1.0$, $St = 1.0$) jet versus Reynolds number (other parameters are $\alpha = 2.0$ and $r_0/\delta = 2.825$).

Sykes and Lyell (1994) and Parthasarathy, 1995). In general, the phase velocity did not vary much with the other parameters (i.e., St, Z) and will not be included in subsequent plots.

The growth rate as a function of wave number with a fixed mass loading ($Z = 1.0$) but different particle inertial parameters is shown in Fig. 7. The single-phase, or one-way coupling, case is also shown in the figure. The destabilization effect at small Stokes number ($St = 0.01$) is again illustrated, since the growth rate for this case is always higher than the one-way coupling case. The most unstable wave number is in the range 2.0–2.5, except for $St = 1.0$, which is about 1.5. For a spatially evolving jet, our results of Figs. 6 and 7 would imply that the most unstable frequency decreases with increasing loading, but almost independent of the Stokes number. The particles with Stokes number on the order 1 are again found to have the strongest stabilization effect on the flow. This effect is better illustrated by plotting the same data as a function of St, as shown in Fig. 8. In Fig. 9, the growth rate for $\alpha = 1.0$ and 2.0 are shown in more detail, along with the single-phase growth rate for each wave number. In addition to showing the highest level of stabilization at a Stokes number on the order of 1, it can also be seen that the particles start destabilizing the

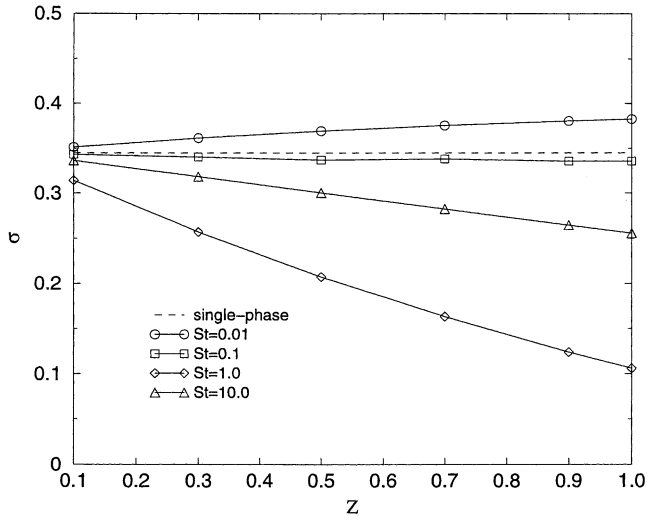

Fig. 5. Growth rate as a function of mass loading with different Stokes numbers ($\alpha = 2.0$, $Re = 500$, and $r_0/\delta = 2.825$).

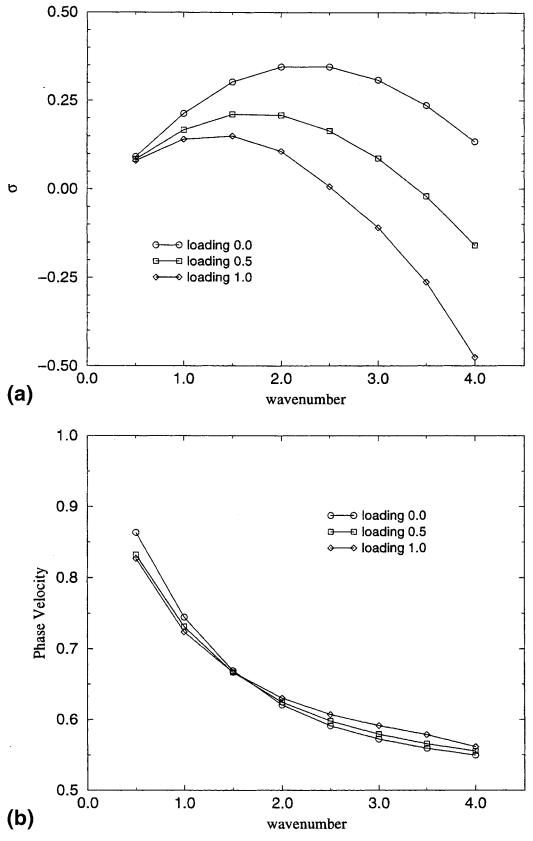

Fig. 6. Growth rate (a) and phase velocity (b) as a function of wavenumber at different mass loading ($Re = 500$, $St = 1.0$, and $r_0/\delta = 2.825$).

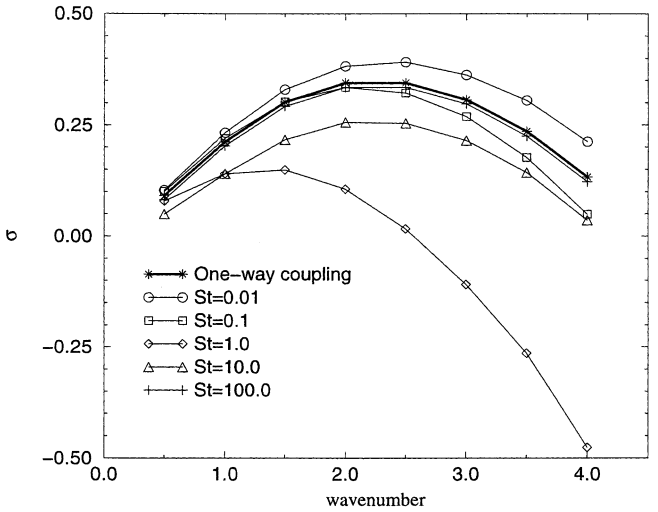

Fig. 7. Growth rate as a function of wavenumber at different Stokes number ($Re = 500$, $Z = 1.0$, and $r_0/\delta = 2.825$).

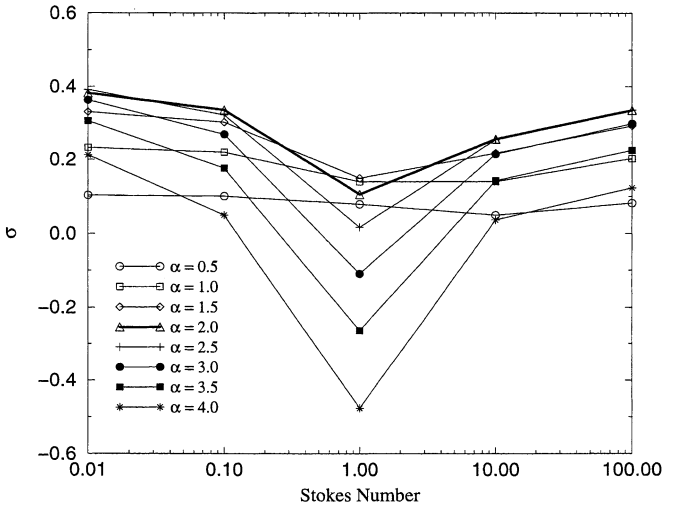

Fig. 8. Growth rate as a function of Stokes number at different wavenumbers ($Re = 500$, $Z = 1.0$, and $r_0/\delta = 2.825$).

flow at a Stokes number of about 0.1 and below. The growth rate of the particle-laden flow approaches that of the single-phase flow for very high Stokes number. The results shown in Figs. 4–9 are very similar to the results for the mixing layer shown by Tong and Wang (1999).

So far we have focused on the amplification rate of flow instability. The linear instability eigenfunctions can be used to give a qualitative description of the flow structure and particle–fluid interaction, as shown in Fig. 10, where the perturbed gas vorticity field, the particle velocity divergence, and perturbation concentration fields are presented. The large-scale roll-up vortex, similar to the single-phase jet, will be formed at the center of the domain as the shear layer is broadened. The particulate velocity field is not divergence free but has a positive divergence in the

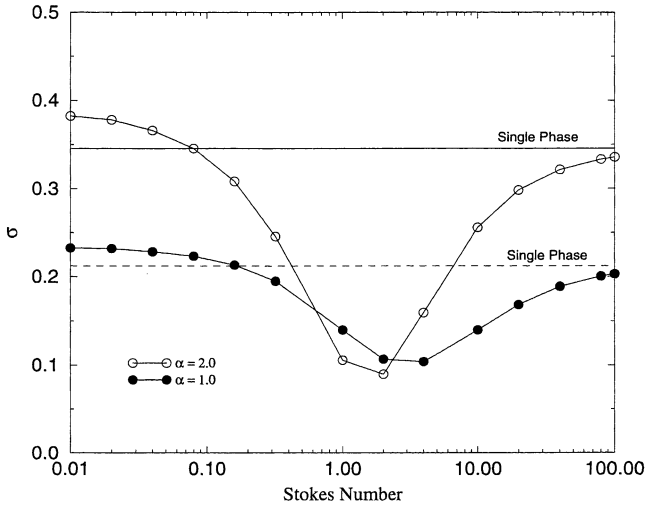

Fig. 9. Growth rate as a function of Stokes number for $\alpha = 1.0$ and 2.0 ($Re = 500$, $Z = 1.0$, and $r_0/\delta = 2.825$).

vortex center and negative divergence in the braid regions, leading to the depletion of particles in the core and accumulation of particles in the braid regions. This preferential accumulation is known for one-way coupled flow, but appears to be qualitatively similar in the two-way coupled case. The level of accumulation is expected to be reduced in the two-way coupled case as the growth rate is significantly reduced for St on the order of 1.

4.4. Comparison with Saffman's asymptotic results

We now compare the numerical results with Saffman's asymptotic prediction at large St, Eq. (17). This result is shown in Fig. 11 for wave numbers 1.0 and 2.0. There is very good agreement when St is on the order of 100. Agreement is also better for large α, as the flow timescale based on the wavelength is decreased.

The comparison of the numerical results with Saffman's prediction at the small St limit ($St = 0.01$) is shown in Fig. 12. Accurate numerical growth rates are harder to obtain because smaller time steps must be used. However, the destabilizing effect is confirmed and approximately follows the predicted dependence on the mass loading from Eq. (16). The effect of Eq. (16) is better illustrated in Fig. 13. The three horizontal lines represent the single-phase flow growth rates at the indicated Reynolds numbers. For a loading of 1.0, the particle-laden growth rate approaches that for a single-phase flow at $Re = 1000$ and for a loading of 3.0, it approaches the single-phase growth rate for a $Re = 2000$ $[Re_e = (1 + Z)Re]$. The cross-over of the curves with respect to the σ_0 ($Re = 500$) horizontal line in Fig. 13 shows that particles with $St < 0.08$ show destabilizing effect while particles with $St > 0.08$ give stabilizing influence for the loadings investigated. The cross-over point is the point where the destabilization effect due to the increase of effective inertia of the fluid–particle mixture balances, in terms of St number, the stabilization effect due to enhanced viscous dissipation around particles. An alternative interpretation of these competing effects in terms of interphase energy transfer can be found in Tong and Wang (1999)

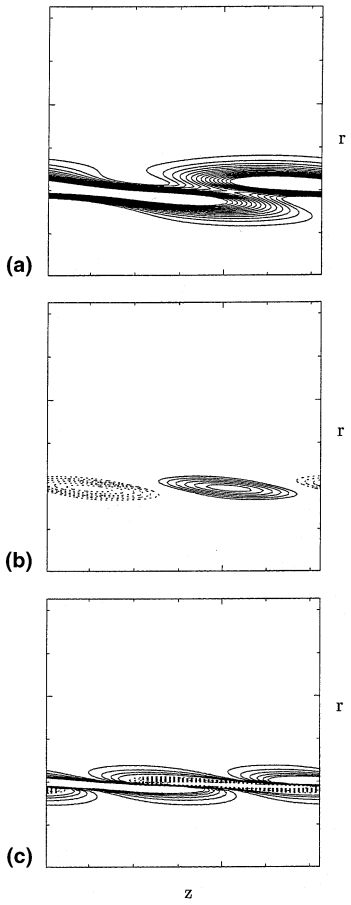

Fig. 10. Visualizations of gas vorticity (a), particle velocity divergence (b), and perturbation concentration (c) fields with $\alpha = 2.0$, $Re = 500$, $St = 1.0$, $Z = 1$, and $r_0/\delta = 2.825$.

for the mixing layer flow. They found that while the gas phase lost energy as a result of augmented viscous dissipations due to the addition of particles at intermediate to large St numbers, the gas phase can gain energy from the particulate phase at small St numbers. Given the qualitatively similar results for the jet and mixing layer, we expect to find the similar interphase energy transfer pattern in particle-laden jets.

5. Summary

We have performed a stability analysis of a temporally evolving particle-laden jet, through numerical simulations equivalent to solving the Orr–Sommerfeld equation of the two-phase flow. The novel solution scheme of Verzicco and Orlandi (1996) has been successfully extended to particle-laden flows in cylindrical coordinates, allowing a study of both linear instability in this paper and non-linear instability in the future.

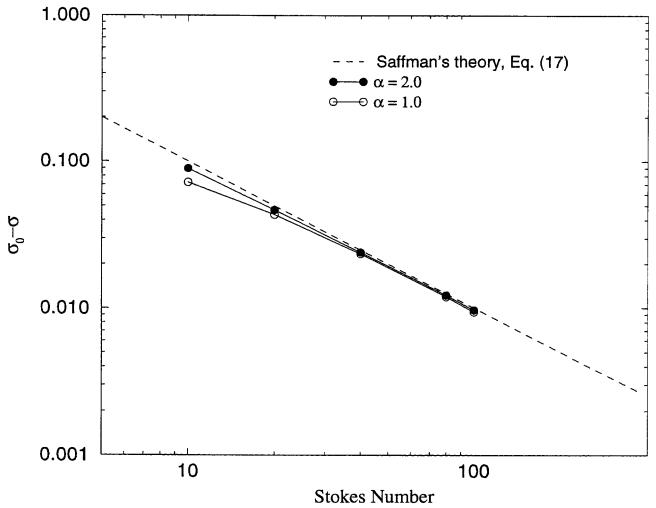

Fig. 11. Comparison of the numerical results with Saffman's theory at the large Stokes number limit ($Re = 500$, $Z = 1.0$, and $r_0/\delta = 2.825$).

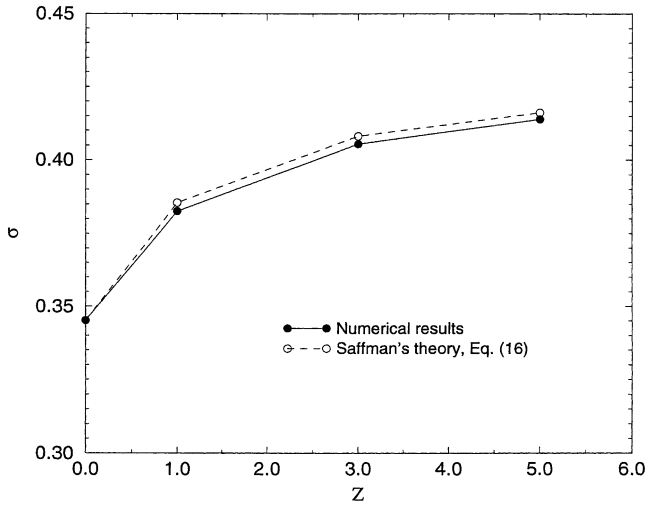

Fig. 12. Comparison of the numerical results with Saffman's theory at the small Stokes number limit ($St = 0.01$) with $Re = 500$, $\alpha = 2.0$, and $r_0/\delta = 2.825$.

Our study extends the work of Tong and Wang (1999) on the stability of the particle-laden mixing layer. In addition to Reynolds number, wave number, particle Stokes number and mass loading, the jet flow stability is complicated by an additional curvature parameter, the ratio of jet radius to shear layer thickness. Furthermore, the wave velocity will vary with these parameters. Nevertheless, we have demonstrated that the following similar scenario holds for a particle-laden

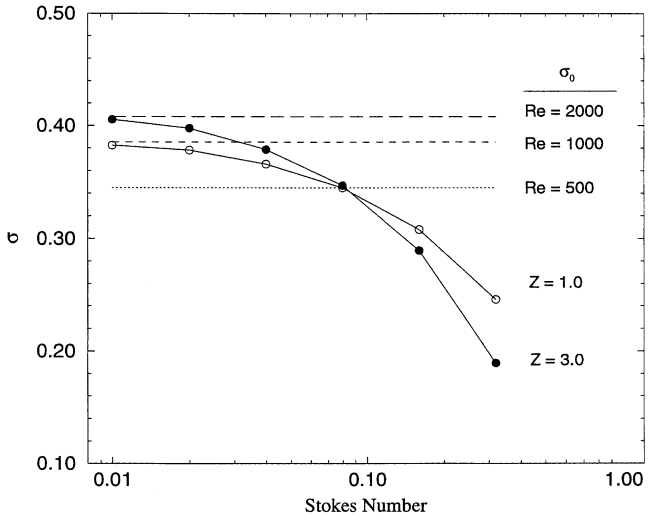

Fig. 13. Comparison of the numerical results with Saffman's theory at the small Stokes number limit ($St = 0.01$) with $Re = 500$, $\alpha = 2.0$, and $r_0/\delta = 2.825$.

jet: the addition of particles can destabilize the flow at small particle Stokes number, while the stabilizing effect prevails for intermediate to large Stokes numbers. Both these competing effects scale approximately linearly with the particle mass loading. Consistent with the results of Sykes and Lyell (1994) and Parthasarathy (1995), we found that the addition of particles increases the wave velocity at large perturbation wave numbers but decreases the wave velocity for long-wave perturbations.

The fact that the addition of particles can destabilize the gas flow in the absence of gravity has been shown to follow the original speculation of Saffman (1962). Two general asymptotic relations proposed by Saffman have been confirmed numerically for the case of the particle-laden jet. Physically, the increase of effective inertia of the fluid–particle mixture causes a destabilization effect while the enhanced viscous dissipation around the particles gives a stabilization effect. Results for various mass loadings, Stokes numbers, and wave numbers show that for a given mass loading and wave number, there is an intermediate Stokes number that corresponds to a maximum flow stability. We have shown that this Stokes number is on the order of 1 and depends weakly on the wave number.

While the stabilizing effect of particles on the mixing layer (Michael, 1965; Yang et al., 1990; Dimas and Kiger, 1998) and jet (Sykes and Lyell, 1994; Parthasarathy, 1995) has been well recognized, the destabilizing influence at small Stokes number discussed here and in Tong and Wang (1999) is realized only for viscous shear flows. It should be noted that with the addition of gravity, particles can introduce buoyancy effects which can destabilize the flow easily (Herbolzheimer, 1983; Shaqfeh and Acrivos, 1986; Borhan and Acrivos, 1988). The qualitatively different effects of the addition of the particles on the flow instability may also be explained in terms of the particle dissipation and effective system inertia, as well as the direction of the interphase energy transfer (e.g., Tong and Wang, 1999).

References

Aggarwal, S.K., 1994. Relationship between Stokes number and intrinsic frequencies in particle-laden flows. AIAA J. 32, 1322–1325.

Aggarwal, S.K., Uthuppan, J., 1999. Particle dispersion enhancement in the near region of a forced jet. J. Propulsion Power 15, 266–271.

Borhan, A., Acrivos, A., 1988. The sedimentation of nondilute suspensions in inclined settlers. Phys. Fluids 31, 3488–3501.

Brancher, P., Chomaz, J.M., Huerre, P., 1994. Direct numerical simulations of round jets – vortex induction and side jets. Phys. Fluids 6, 1768–1774.

Chung, J.N., Troutt, T.R., 1988. Simulation of particle dispersion in an axisymmetric jet. J. Fluid Mech. 186, 199–222.

Crowe, C.T., Chung, J.N., Troutt, T.R., 1988. Particle mixing in free shear flows. Prog. Energy Combust. Sci. 14, 171–194.

Crowe, C.T., Chung, J.N., Troutt, T.R., 1993. Particle dispersion by organized turbulent structures. In: Roco, M.C. (Ed.), Particulate Two-phase Flows. Butterworth-Heinemann, New York (Chapter 18).

Crowe, C.T., Sommerfeld, M., Tsuji, Y., 1997. Multiphase Flows with Droplets and Particles. CRC Press, Boca Raton, FL.

Dimas, A.A., Kiger, K.T., 1998. Linear instability of a particle-laden mixing layer with a dynamic dispersed phase. Phys. Fluids 10, 2539–2557.

Eaton, J.K., Fessler, J.R., 1994. Preferential concentration of particles by turbulence. Int. J. Multiphase Flow 20 (Suppl.), 169–209.

Elghobashi, S., 1994. On predicting particle-laden turbulent flows. Appl. Sci. Res. 52, 309–329.

Elghobashi, S., Truesdell, G.C., 1993. On the two-way interaction between homogeneous turbulence and dispersed solid particles. I: turbulence modulation. Phys. Fluids A 5, 1790–1801.

Glaze, D.J., Frankel, S.H., 2000. Effect of dispersion characteristics on particle temperature in an idealized nonpremized reacting jet. Int. J. Multiphase Flow 26, 609–633.

Gore, R.A., Crowe, C.T., 1989. Effect of particle-size on modulating turbulent intensity. Int. J. Multiphase Flow 15, 279–285.

Gore, R.A., Crowe, C.T., 1991. Modulation of turbulence by a dispersed phase. ASME J. Fluid Eng. 113, 304–307.

Hansell, D., Kennedy, I.M., Kollmann, W., 1992. A simulation of particle dispersion in a turbulent jet. Int. J. Multiphase Flow 18, 559–576.

Herbolzheimer, E., 1983. Stability of the flow during sedimentation in channels. Phys. Fluids 26, 2043–2054.

Hetsroni, G., 1989. Particle-turbulence interaction. Int. J. Multiphase flow 15, 735–746.

Huerre, P., Monkewitz, P.A., 1985. Absolute and convective instabilities in free shear layers. J. Fluid Mech. 159, 151–168.

Kim, J., Moin, P., 1985. Application of a fractional-step method to incompressible Navier–Stokes equations. J. Comput. Phys. 59, 308–323.

Liu, J.T.C., 1989. Ann. Rev. Fluid Mech. 21, 285–315.

Longmire, E.K., Eaton, J.K., 1992. Structure of particle-laden round jet. J. Fluid Mech. 236, 217–257.

Martin, J.E., Meiburg, E., 1991. Numerical investigation of 3-dimensionally evolving jets subject to axisymmetrical and azimuthal perturbations. J. Fluid Mech. 230, 271–318.

Michael, D.H., 1965. Kelvin–Helmholtz instability of a dusty gas. Proc. Camb. Philos. Soc. 61, 569–571.

Michalke, A., 1984. Survey on jet instability theory. Prog. Aerospace Sci., 159–199.

Monkewitz, P.A., Pfizenmaier, E., 1991. Mixing by side jets in strongly forced and self-excited round jets. Phys. Fluids A 3, 1356–1361.

Morris, P.J., 1976. Spatial viscous instability of axisymmetric jets. J. Fluid Mech. 77, 511–529.

Parthasarathy, R.N., 1995. Stability of particle-laden round jet to small disturbances. In: Proceedings of the FEDSM '95, vol. 228, pp. 427–434.

Rai, M.M., Moin, P., 1991. Direct simulations of turbulent-flow using finite-difference schemes. J. Comput. Phys. 96, 15–53.

Saffman, P.G., 1962. On the stability of laminar flow of a dusty gas. J. Fluid Mech. 13, 120–128.

Shaqfeh, E.S.G., Acrivos, A., 1986. The effects of inertia on the stability of the convective flow in inclined particle settlers. Phys. Fluids 30, 960–973.

Slater, S.A., Young, J.B., 1998. The calculation of inertial particle transport using an Eulerian formulation. In: Proceedings of the FEDSM '98, vol. 245.

Squires, K.D., Eaton, J.K., 1990. Particle response and turbulence modification in isotropic turbulence. Phys. Fluids A 2, 1191–1203.

Sykes, D., Lyell, M.J., 1994. The effect of particle loading on the spatial stability of a circular jet. Phys. Fluids 6, 1937–1939.

Tong, X.-L., Wang, L.-P., 1999. Two-way coupled particle-laden mixing layer. Part 1: Linear instability. Int. J. Multiphase Flow 25, 575–598.

Uthuppan, J., Aggarwal, S.K., Grinstein, F.F., Kailasanath, K., 1994. Particle dispersion in a transitional axisymmetrical jet – a numerical simulation. AIAA J. 32, 2004–2014.

Verzicco, R., Orlandi, P., 1996. A finite-difference scheme for three-dimensional incompressible flows in cylindrical coordinates. J. Comput. Phys. 123, 402–414.

Wen, F., Evans, J., 1994. Linear instability of a two-layer flow with differential particle loading. Phys. Fluids 6, 3893–3905.

Yang, Y.Q., Chung, J.N., Troutt, T.R., Crowe, C.T., 1990. The influence of particles on the spatial stability of two-phase mixing layers. Phys. Fluids 2, 1839–1845.

Yarin, L.P., Hetsroni, G., 1994. Turbulence intensity in dilute two-phase flows. 3. The particles–turbulence interaction in dilute two-phase. Int. J. Multiphase flow 20, 27–44.

Yuan, Z., Michaelides, E.E., 1992. Turbulence modulation in particulate flows – a theoretical approach. Int. J. Multiphase flow 18, 779–785.